Aggregation-Enhanced Raman Scattering of a Cyanine Dye in Homogeneous Solution

Daniel L. Akins,* Serdar Özçelik, Han-Ru Zhu, and Chu Guo

Center for Analysis of Structures and Interfaces (CASI), Department of Chemistry, The City College of The City University of New York, New York, New York 10031

Received: October 10, 1996; In Final Form: January 2, 1997[⊗]

We have conducted Raman investigations on the cyanine dye 3,3′-dimethyl-9-phenyl-4,5:4′,5′-dinaphthothiacarbocyanine (NTC) for which an enhanced Raman scattering occurs that is concomitant with the formation of aggregates, and for which resonance Raman and surface-enhanced Raman scattering can be excluded. The formation of aggregated molecules is determined through characteristic changes in absorption and fluorescence spectra. Also, fluorescence lifetime measurements for monomeric and aggregated NTC are reported and independently confirm aggregate formation. Off-resonance Raman measurements for NTC in various physical states confirm that molecular aggregation leads to an enhancement of Raman scattering of vibrational modes of the monomeric species (i.e., intramolecular modes) and an even greater relative enhancement of certain modes of the molecules involved more intimately with formation of the aggregate (i.e., intermolecular modes). Additionally, we make empirical band assignments for NTC from which we are able to exclude structural distortion due to intermolecular interaction as the source for Raman band intensity enhancement.

I. Introduction

The structure and optical dynamics of molecular aggregates are subjects of intense interest. At its most basic level, interest in molecular aggregates derives from the opportunity such structures provide to study intermolecular interactions with reduced degrees of freedom. At its most sophisticated level, interest in aggregates derive from the realization that aggregated molecules play crucial roles in nature; indeed, processes upon which life itself depends, such as light-harvesting and the primary charge-separation steps in photosynthesis, are facilitated by aggregated species.[1−4] Moreover, molecular aggregates have important current and potential technological applications. For example, aggregates formed of molecular dyes have been used as spectral sensitizers (principally for silver halide semiconductor materials),[5] as organic photoconductors,[6] as optical probes in biological and synthetic membrane systems,[7] as photopolymerization initiators,[8] and, because of their enhanced nonlinear optical susceptibilities,[9,10] as materials for use in nonlinear optical devices.[11−13]

The primary mechanism through which molecular aggregate structures in both natural and artificial systems are created is self-assembly through intrinsic intermolecular interactions; aggregates form in homogeneous solution and on surfaces (such as on an electrode), as well as on interfaces of artificial bilayers and native membranes. Often such self-assembled molecular aggregates can be classified as being of J- or H-type, defined by the relative orientations of induced transition dipoles of the constituent molecules, either "head-to-tail" or "head-to-head," respectively.[14] Molecules whose aggregates can be qualitatively described by this picture include dyes such as the cyanines[15−26] and the xanthenes,[27−29] polycyclic aromatics,[30−35] and, recently, N-protonated porphyrins.[36−38] Such structural pictures provide a simplistic framework for theoretical analysis of structure and emission dynamics of electronically excited aggregated systems.

The molecular exciton model that enables the characterization of aggregates as J or H utilizes the quantum mechanical precept that electronic energy is not localized in any particular molecule in the molecular aggregate, and interactions between induced transition dipole moments that are distributed throughout the aggregate structure (as a result of superposition of states) create an electronic band of states that pertain to movement of electrons over the entire spatial expanse of the aggregate.[14] More recent extensions of the basic molecular exciton concept have incorporated effects of intermolecular vibronic coupling and exciton−phonon interaction, as well as inhomogeneous environmental effects on aggregate spectral and fluorescence emission properties.[39−42] The molecular exciton model is successful in explaining, among other things, absorption band frequency shifts and absorption band narrowing, as well as selection rules for electronic transitions between different excitonic states.[14]

More detailed architectures for molecular aggregates than required for designation as J- or H-type have been suggested. These include arrangements that are defined as "staircase",[43] "herringbone",[44] "cofacial",[45] and "brickwork".[46] But, in fact, all such designations derive from insights provided by spectroscopic techniques that are of insufficient resolution to provide information about the structure of the constituent molecules that compose the aggregate or, for that matter, the specific nature of the intermolecular interactions between the constituent molecules. Indeed, much about structure is inferred from chemical intuition.

More recently, we have suggested for 1,1′-diethyl-2,2′-cyanine (referred to also as pseudoisocyanine, PIC; see Figure 1) that all-trans and mono-cis stereoisomers, which pertain to rotation of quinoline groups about the methine chain of the cyanine dye, independently form two types of J aggregates.[47] We have relied heavily on vibrational Raman measurements to arrive at our description of the J-aggregate and have advanced a theory of enhancement of Raman scattering associated with the existence of the aggregate (i.e., "aggregation enhanced Raman scattering", referred to also as AERS). In our approach, molecular exciton concepts were incorporated into the Raman scattering problem and resulted in a quantum theory derived analytic intensity expression—based on a different enhancement mechanism than

[⊗] Abstract published in *Advance ACS Abstracts,* April 15, 1997.

S1089-5639(96)03122-2 CCC: $14.00

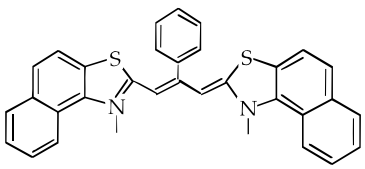

NTC

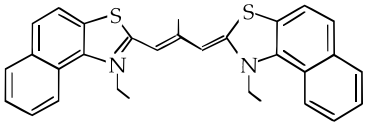

mNTC

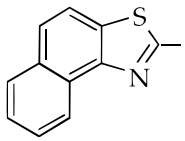

NmTA

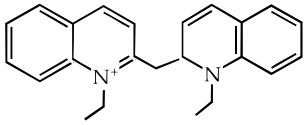

PIC

Figure 1. Structures of cyanine dyes and reference compounds.

that used for surface-enhanced Raman scattering (SERS)—that explains the enhancement of vibrational Raman band intensities for aggregated molecules in terms of an increased-size effect and near resonance terms in the polarizability.[19,20] The former effect is associated with the polarizability of the aggregate resulting from the additivity of single molecule polarizabilities, while for all but a small number of "broad" low-frequency bands, the latter is attributable to small energy separations between the molecular aggregate electronic state[14,36,37] (viz., the molecular excitonic state) and other electronic states.[19,20]

With regard to optical dynamics of excitonic states, it is to be noted that this area of research has become extremely active in recent years.[48−52] Topics such as superradiance, nonradiative relaxation, nonlinear optical response, etc. dominate the literature dealing with aggregated molecules. As in the case of structure issues, the optical dynamics of aggregates can be addressed through exciton concepts, where coupled molecules cooperatively participate in the emission process. As with aggregate structure issues, most studies have focused on cyanine dyes.

In this paper we conduct Raman investigations on a cyanine dye for which enhancement of Raman scattering is concomitant with the formation of aggregates, and for which resonance Raman enhancement and SERS can be excluded. This work is interpreted as providing strong evidence that the AERS mechanism is operative: earlier studies from this laboratory, involving Raman enhancement upon formation of the aggregate for other cyanine dyes adsorbed onto surfaces,[22−26,47] as well as for tetrakis(*p*-sulfonatophenyl)porphyrin (TSPP) in acidic, homogeneous solution have also provided supporting evidence.[36−38] The specific molecule studied in this paper is 3,3′-dimethyl-9-phenyl-4,5:4′,5′-dinaphthothiacarbocyanine, hereinafter referred to as NTC; see Figure 1.

Additionally, we make empirical band assignments for NTC, arrived at through the use of homologous dyes, from which we are able to exclude structural distortion due to intermolecular interaction as the source for Raman band intensity enhancement, and, furthermore, associate vibrational modes that are enhanced with the architecture of the aggregate.

II. Experimental Section

The focus of this study is the cyanine dye NTC with chloride as the counterion. Other compounds used in this study to aid in empirical assignments of the Raman bands of NTC are 3,3′-diethyl-9-methyl-4,5:4′,5′-dinaphthothiacarbocyanine (mNTC) and 2-methyl-4,5-naphthothiazole (NmTA); structures are provided in Figure 1.

NTC was purchased from Nippon Kanko Shikiso Co., Ltd., of Okayama, Japan. The other compounds were purchased from the Eastman Kodak Chemical Co., Rochester, NY. All spectroscopic measurements were conducted at room temperature.

Solutions were prepared by dissolving a specific compound in an appropriate solvent, specifically, spectral grade methanol, deionized water, or their mixture. The concentration in experiments dealing with monomeric dyes was kept sufficiently low (ca. 5×10^{-6} M) that no aggregation occurred. In studies dealing with aggregates, the dye concentration was increased to the range $(1-2) \times 10^{-4}$ M. The presence of the aggregate was determined through the appearance of a narrow, red-shifted absorption band, characteristic of aggregate formation, by absorption measurements using a Perkin-Elmer UV/vis/NIR spectrometer, Model Lambda-19. Additional evidence for aggregate formation was provided through the observation of pseudoresonance fluorescence, which was acquired using a SPEX Fluorolog-τ2 spectrofluorometer. This latter instrument also enables fluorescence lifetime measurements by the phase modulation method, which allows low-intensity incandescent or laser CW excitation to be used as the excitation source.

Emission lifetimes of monomeric and aggregated NTC were obtained from fluorescence decay measurements. Fluorescence of the NTC solution in square quartz cuvettes was excited at a wavelength close to the dye's absorption maximum (specifically, $\lambda_f^{max} = 635$ nm). Excitation pulses of ca. 5 ps duration and peak power at the sample of 35 mW (0.46 nJ/pulse; ~230 kW/pulse) were provided by a DCM dye laser (Coherent 700) pumped by a Coherent Antares 76s mode-locked Nd:YAG laser. Fluorescence decay was captured by a Hamamatsu streak camera, Model C4334, optically coupled to a charge-coupled-device (CCD) array detector. This system allows measurements of both the temporal profile and the resolved emission spectrum (in combination with a dispersive spectrometer). The time resolution that we attained with this system, using Hamamatsu U4290 fluorescence analysis software, is estimated to be better than 10 ps.

In parallel with streak camera measured emission lifetime measurements, phase-modulation emission rates were also made. These measures were principally made to ensure that incident laser intensities were sufficiently low that exciton annihilation did not influence emission dynamics. For the phase modulation technique a SPEX Fluorolog-τ2 spectrofluorometer (that uses low-intensity cw excitation) was used. A significant difference between the lifetimes measured using the two techniques led to the use of lower laser intensity.

Raman spectra of cyanine dyes on smooth as well as roughened silver electrode surfaces and in the polycrystalline state were recorded as previously described in detail.[22,24,53] Raman spectra of NTC in homogeneous solutions were excited at off-resonance wavelengths: specifically, the Raman spectrum of monomeric NTC in methanol solution was excited at 514.5 nm using radiation from a Coherent Innova 200 argon ion laser; the off-resonance Raman spectrum of aggregated NTC in a methanol/water solvent was excited at 730 nm using radiation

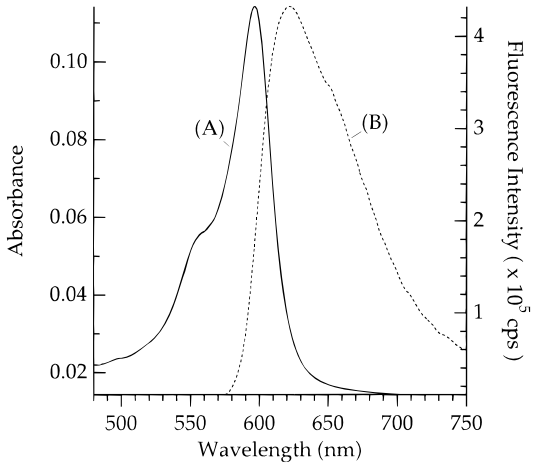

Figure 2. (A) absorption and (B) fluorescence spectra of monomeric NTC in methanol. NTC concentration ca. 10^{-6} M. Fluorescence excited using excitation at 550 nm.

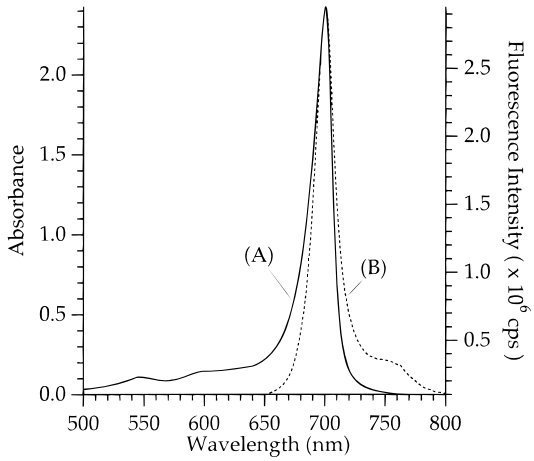

Figure 3. (A) absorption and (B) fluorescence spectra of monomeric NTC in methanol−water mixed solvent (1:9 by volume). NTC concentration ca. 10^{-6} M. Fluorescence excited at 635 nm.

from a Ti:sapphire laser (Coherent 899 ring-laser) pumped by a Coherent Innova 200 argon ion laser.

Raman spectra were recorded using a SPEX 1877, 0.6-m triple-spectrometer, coupled to a CCD detector (Spectrum-1) cooled to 140 K with liquid nitrogen. Excitation power in Raman experiments were maintained at ca. 20 mW. Additionally, for the polycrystalline sample a Bomem FT-Raman spectrometer (Model DA 3.16) was used, which we have utilized for several other studies and described thoroughly.[24,53] A Quantronix Model 114 Nd:YAG laser of wavelength 1.064 μm was the excitation source. All Raman spectra reported here have been refined by background subtraction—by exporting files to analysis software (Igor) from Wavematrics (Lake Oswego, Oregon)—and have a spectral resolution of ca. ± 2 cm^{-1}.

III. Results

A. Absorption and Fluorescence Spectroscopy of NTC Monomer and Aggregate. The electronic absorption spectrum of NTC in methanol is shown in Figure 2. This spectrum exhibits a broad $0 \leftarrow 0$ vibronic band at 595 nm with a weak "shoulder" near 548 nm, associated with the $1 \leftarrow 0$ vibronic transition. The spectral pattern exhibited in Figure 2 does not change with increase in the concentration of NTC in methanol up to 10^{-3} M. However, addition of water is found to promote the emergence of two additional absorption bands, one at 548 nm and the other at 700 nm. These latter bands grow at the expense of the 595 nm monomer absorption, and their positions are only weakly dependent on the concentration of NTC. Increasing NTC concentration is found to cause a decrease in the intensity of the high-frequency band at 548 nm, while the red-shifted band at 700 nm experiences a dramatic intensity enhancement and a significant bandwidth narrowing, i.e., from $\Delta\nu = 721$ cm^{-1} for methanol solvent to $\Delta\nu = 470$ cm^{-1} for a water−methanol solution; see Figure 3.

The above-mentioned spectral changes that occur when water is added to methanol are indicative of aggregate formation, as exemplified by changes in the absorption spectrum of PIC when aggregates are formed under various conditions.[16] The red-shifted absorption band that occurs for NTC is attributed to the aggregate, and the blue-shifted band, which diminishes as the red-shifted band experiences an intensity increase, is probably due to NTC dimer.

Figures 2 and 3 also show fluorescence spectra of NTC (dashed lines) in methanol and in water−methanol solvents, respectively. The broad fluorescence in Figure 2 with a fluorescence maximum at ca. $\lambda_f^{max} = 620$ nm, of bandwidth ($\Delta\nu_{fl} = 843$ cm^{-1}), is due to the emission from the lowest excited electronic state of monomeric NTC; the sharper fluorescence band in Figure 3 ($\Delta\nu_{fl} = 490$ cm^{-1}) is attributable to aggregated NTC. It was observed that the frequency separation between the fluorescence maximum λ_f^{max} and the absorption maximum λ_a^{max}, for the putative aggregate system, is concentration dependent and becomes negligible when the NTC concentration is increased to ca. 10^{-4} M. We might note that the concentration dependent frequency difference between the two maxima is likely associated with a change in the number of NTC molecules involved in the aggregate with change in NTC concentration.

Upon combining both the electronic absorption and fluorescence spectral evidence, one can confidently conclude that NTC molecules aggregate when water is added to a methanol solution and the number of NTC molecules cooperatively coupled in the aggregate increases with NTC concentration increase.

B. Fluorescence Lifetimes of Monomeric and Aggregated NTC. Typical fluorescence decay curves of NTC in methanol and in a methanol−water solvents (1:9 by volume) are shown in Figure 4. These decay profiles were determined using the streak camera system mentioned earlier and are best fit by a single exponential relaxation expression ($\chi^2 = 1.5$ for the aggregate and 0.9 for the monomer). Fluorescence lifetimes of monomeric NTC in alcoholic solvents are found to vary only slightly with solvent polarity, but decrease dramatically with decreasing viscosity of the solvent, as shown in Table 1.

The dependence of fluorescence lifetime of the monomer on solvent viscosity can be rationalized in terms of a change in the barrier to molecular torsion within the NTC monomer, with a concomitant altering of nonradiative rates. Indeed, as mention earlier, the existence of stereoisomers (as well as photoisomers) are known to affect fluorescence lifetimes of the cyanine dyes.[54−62]

Also indicated in Table 1 is a measurement that shows that the fluorescence lifetime of NTC is considerably lowered upon addition of water. This observation is consistent with the observation of lifetime shortening in the case of pseudoisocyanine (PIC)[51] as well as porphyrin[38,63] when aggregates are formed, and provides further experimental support for the presence of aggregated NTC.

It is to be noted that fluorescence from aggregated molecules is widely understood as resulting from radiative decay (relaxation) of coherently coupled molecules and, moreover, the physical number of molecules in an aggregate can be substan-

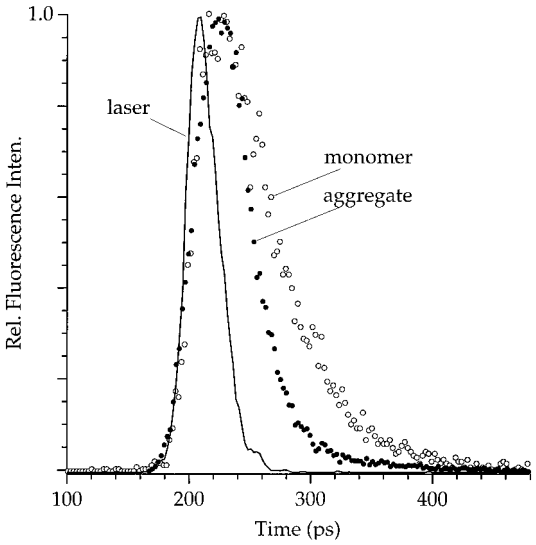

Figure 4. Fluorescence decay curves of NTC: (A) monomer, open circle; (B) aggregate, closed circle; and (C) excitation pulse profile, solid curve. Samples are the same as those used for Figures 1 and 2. Wavelengths at which fluorescence decay were monitored were 620 and 700 nm for the monomer and aggregate, respectively. Displayed decay curves required 100 scans to acquire.

TABLE 1: Fluorescence Lifetime (τ_{fl}) Data of Monomeric and Aggregated NTC in Different Solvents[a]

solvent	polarity E_I (30)[b]	viscosity (cP)	τ_{fl} (ps) phase mod	τ_{fl} (ps) streak cam
methanol	55.5	0.597	55 ± 5	40.9 ± 0.4
ethylene glycol	56.3	19.9	387 ± 15	396.5 ± 2
glycerol	57.0	1490.0	1994 ± 15	1659.0 ± 8
methanol−water (1:9 by volume)		1.33		18.5 ± 0.2

[a] Measured using both the phase modulation and streak camera techniques. [b] See ref 77.

tially larger than the number of molecules that coherently emit. This latter concept leads to the defining of an effective number of coupled molecules, termed the coherence size or number, represented as N_{eff}, and as a result of the cooperation, the radiative rate of the aggregate is expected to be N_{eff} times faster (in simple exciton theory) than that for the isolated single molecule.

Furthermore, early determinations of emission parameters for aggregates, whether fluorescence lifetimes or quantum yields, photon echo relaxation times, etc., led to an appreciation of the influence of incident laser power induced exciton−exciton annihilation effects on measured values of the parameters. Fluorescence lifetime of J-aggregates formed in solution or in a low-temperature glass were typically extremely short,[64−68] on the order of tens of picoseconds. However, Sundström *et al.*[69] performed experiments on J-aggregates of PIC in homogeneous aqueous solution at room temperature and ascertained that both the lifetime and the fluorescence yield were significantly influenced by excitation pulse intensity; a single, limiting exponential lifetime of about 400 ps was measured at low excitation intensity.

As a result of this latter finding, as mention earlier, we have adjusted the incident intensity used in our streak camera measurements by comparison of measured fluorescence lifetimes with the lifetimes determined using the phase modulation technique, which are not influenced by high exciton density.[38]

C. Raman Spectra of Monomeric and Aggregated NTC. Figure 5 provides off-resonance Raman spectra of NTC in various physical states. Part A shows the spectrum for aggregated NTC in water−methanol homogeneous solution with $\lambda_{ex} = 730$ nm. Part B provides the spectrum for the dye adsorbate onto a smooth silver electrode surface. This latter spectrum is clearly very similar to that of the solution aggregate, even though $\lambda_{ex} = 514.5$ nm, with the principal difference being the relative intensities of the two bands below 200 cm^{-1}. Part C provides the spectrum for the dye adsorbed onto roughened silver electrode surfaces with $\lambda_{ex} = 514.5$ nm. For this spectrum the pretreatment of the electrode was conducted prior to insertion of the dye into the electrochemical cell, as has been described in an earlier publication from this laboratory.[70]

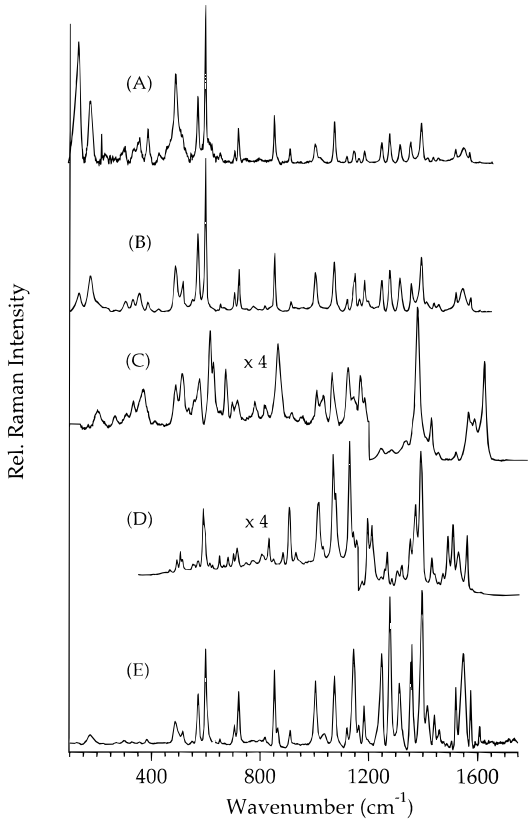

Figure 5. Raman spectra of NTC acquired using different conditions. (A) Off-resonance Raman spectrum of aggregated 10^{-4} M NTC excited at 730 nm in methanol−water (1:9 by volume) mixed solvent. (B) Off-resonace Raman spectrum of NTC adsorbed onto a smooth silver electrode surface in a 1:9 (by volume) methanol-water solution with potential set at −0.6 V vs SCE, excitation wavelength 514.5 nm, and KCl concentration of 0.1 M. (C) Surface-enhanced Raman spectrum of NTC adsorbed onto a roughened silver electrode at a potential of −0.6 V vs SCE and with 0.1 N KCl as supporting electrolyte. Spectra below 1200 cm^{-1} is amplified by a factor of 4 and offset by +4000 cps. Pretreatment of the electrode involved polishing the electrode, followed by sonification, and then oxidizing the electrode at +0.6 V vs SCE and adding dye. The exciting wavelength and power for SERS was 514.5 nm and 50 mW, respectively. (D) FT-Raman spectrum of polycrystalline NTC using 1064 nm excitation. The part of the spectra below 1100 cm^{-1} is amplified by a factor of 4 and offset by +1000 cps. (E) Off-resonance Raman spectrum of monomeric NTC at a concentration of 10^{-4} M excited at 514.5 nm in methanol.

Parts D and E respectively provide the spectra of the polycrystalline solid ($\lambda_{ex} = 1064$ nm) and that of monomeric NTC in methanol ($\lambda_{ex} = 514.5$) for reference purposes. The correlated band positions and relative intensities, as well as their assignments to vibrations of various moieties, for each of the Raman bands shown in Figure 5 are listed in Table 2.

Inspection of various spectra in Figure 5 for the frequency region above ca. 600 cm^{-1} (hereinafter referred to as the high-frequency region) reveals that Raman spectra for monomeric

TABLE 2: Raman Spectral of Monomeric and Aggregated NTC[a]

monomer[b] $\lambda_{ex} = 514.5$ nm	aggregate[c] $\lambda_{ex} = 730$ nm	smooth Ag[d] $\lambda_{ex} = 514.5$ nm	rough Ag[d] $\lambda_{ex} = 514.5$ nm	solid[e] $\lambda_{ex} = 1064$ nm	mode assignment[f]
–	133(3.08)	131(0.36)	–	–	lattice
175(0.05)	176(1.56)	174(0.67)	–	–	int borrowing
–	–	–	202(0.02)	–	–
271(0.01)	–	263 vw?	267(0.01)	–	
299(0.02)	303(0.40)	302(0.22)	309(0.02)	–	int borrowing
328(0.01)	–	328(0.25)	334(0.04)	–	$(ring)_{N-B}$
356(0.01)	357(0.64)	352(0.36)	–	–	Int. borrowing
383(0.02)	387(0.88)	383(0.19)	371(0.06)	–	$(Ring)_{N-B}$
–	427(0.28)	422(0.08)	–	–	
487(0.14)	488(2.28)	484(0.86)	490(0.06)	492(0.03)	C−C in bridge
–	–	–	–	504(0.04)	
–	–	512(0.58)	511(0.08)	512(0.03)	C−C in bridge
570(0.40)	569(1.68)	566(1.44)	577(0.07)	569(0.03)	C−C in bridge
–	–	–	615(0.15)		
597(0.56)	598(3.96)	594(2.78)	602(0.01)	589(0.11)	C−C in bridge
			629(0.10)		
651(0.03)	651(0.28)	649(0.19)	–	648(0.03)	C−C in bridge
			673(0.09)	680(0.03)	
706(0.33)	706(0.32)	700(0.36)	697(0.04)	700(0.04)	C−C in bridge
723(0.33)	719(0.88)	716(0.77)	716(0.04)	714(0.05)	C−C in bridge
–	–	–	781(0.04)	–	
819(0.04)	–	–	819(0.03)	830(0.06)	C−C in bridge
855(0.48)	851(1.20)	848(1.08)	866(0.13)	848(0.04)	C−C in bridge
–	–	–	–	882(0.04)	
912(0.07)	910(0.36)	908(0.22)	918(0.02)	906(0.11)	C−C in bridge
–	–	–	–	929(0.04)	
1006(0.41)	1001(0.48)	997(0.75)	1009(0.06)	1014(0.12)	9−phenyl
–	–	–	1032(0.05)	1029(0.05)	$(ring)_{N-B}$
–	–	1066(0.92)	1065(0.08)	1067(0.20)	C−C in bridge
1076(0.43)	1073(1.04)	–	–	1076(0.14) sh	C−C in bridge
1124(0.10)	1119(0.16)	1115(0.25)	1124(0.09)	1128(0.23)	C−C in bridge
1146(0.64)	1144(0.32)	1142(0.72)	1145(0.04)	1142(0.09) s	$(ring)_{N-B}$
1165(0.12)−	1163(0.12)	1159(0.25)	–	–	C−C in bridge
1185(0.24)	1184(0.32)	1178(0.58)	1168(0.08)	1174(0.12)	C−C in bridge
–	–	–	1184(0.04)	1194(0.54)	$(ring)_N$
–	–	1205(0.22)	–	1210(0.50)	
1248(0.59)	1247(0.52)	1241(0.58)	1243(0.07)	1245(0.14)	
1280(0.39)	1276(0.76)	1270(0.78)	–	1266(0.32)	$(ring)_N$
–	–	–	1283(0.07)	1283(0.13)	
1316(0.41)	1314(0.48)	1308(0.64)	–	1304(0.19)	C−C in bridge
–	–	–	–	1319(0.22)	
1356(0.53)	1353(0.16)	1349(0.53)	1338(0.13)	1350(0.40)	$(ring)_{N-B}$
–	–	–	–	1369(0.64)	
1396(1.00)	1393(1.00)	1385(1.00)	1378(1.00)	1388(1.00)	$(ring)_{N-B}$
1416(0.25)	1414(0.12)	1404(0.22)	–	–	
1442(0.20)	–	1432(0.19)	1429(0.28)	1429(0.28)	$(ring)_N$
–	–	–	–	1440(0.16) sh	
1450(0.08)	1453(0.12)	1449(0.17)	1455(0.05)	1456 vw	
–	–	–	–	1469(0.17) sh	
–	–	–	–	1488(0.42)	
1521(0.37)	1519(0.36)	1512(0.36)	1520(0.05)	1507(0.50)	$(ring)_N$
1548(0.58)	1547(0.40)	1536(0.44)	–	1527(0.32)	$(ring)_{N-B}$
1574(0.29)	1569(0.28)	1565(0.27)	1565(0.31)	1559(0.43)	C−C in bridge
1603(0.16)	1605(0.04)	1599(0.05)	1587(0.27)	1570(0.06)	$(ring)_{N-B}$
–	–	–	1623(0.65)	1609(0.04)	

[a] Dye concentration, ca. 10^{-4} M. [b] Methanol used as solvent. [c] Solvent consisted of 90% (vol) water + 10% (vol) methanol. [d] Solvent consisted of 90% (vol) water + 10% (vol) methanol, KCl used as electrolyte. [e] FT−Raman measurement. [f] Int. borrowing refers to intensity borrowing from the intermolecular (lattice) transition by an intramolecular mode; $(ring)_N$ and $(ring)_{N-B}$ represent, respectively, vibrational modes of the naphthothiazolic ring that are either isolated from or coupled to vibrations (stretching or bending) of the methine chain.

and aggregated NTC (parts E and A of Figure 5, respectively) possess bands of nearly the same frequencies. However, below 600 cm^{-1} (low-frequency region) the two spectra differ substantially, with the aggregate spectrum containing several bands (e.g., 133, 176, 302, and 352 cm^{-1}) that are either not detectable, even upon amplification for better assessment, or quite weak in the monomer's spectrum. Moreover, for the aggregate in homogeneous solution, the bands in the low-frequency region are significantly enhanced relative to the high-frequency bands. A similar relation applies in the case of NTC adsorbed onto a smooth silver electrode (part B of Figure 5), while such is not the case for the homogeneous monomeric system.

An obvious deduction, based on the similarity of the Raman spectra (parts A and B of Figure 5), is that the scattering species adsorbed onto the smooth silver surface, as it is for the species in the homogeneous solution, is aggregated NTC. In general, one might expect a somewhat different structure for an aggregate adsorbed onto a substrate as opposed to dispersed in homogeneous solution—for example, a two-dimensional arrangement, especially for the first monolayer, might be expected for the

adsorbed aggregate, while a three-dimensional geometry throughout might be expected for the solution phase aggregate—unless, of course, a one-dimensional, stringlike configuration is the effective geometry. The almost identical Raman band positions for the two "environments" (see Table 2) would appear to confirm the essential similarity in structures of the scattering species.

The Raman spectrum of NTC adsorbed onto a roughened silver surface, i.e., SERS spectrum (Figure 5, part C), differs substantially from those of the monomer and the aggregate. In particular, bands that are enhanced in relative intensity are not the same ones that are enhanced when the molecule is known to exist in the aggregate state. Moreover, we have found that the SERS spectrum is of lower overall intensity (i.e., lower signal-to-noise). Such a finding is consistent with observations made in this laboratory, where we have found that enhanced Raman scattering on a smooth silver electrode results in a larger signal than that when a roughened surface is used.[22,53] We attributed this difference to the existence of AERS, which is an independent mechanism for the enhancement of Raman intensity and which depends on the presence of aligned molecules at the interface, which is not as facilely attainable for an interface replete with protuberances, characteristic of a SERS active surface.

Lastly, we note that the Raman spectrum of polycrystalline NTC, which does not extend below ca. 400 cm^{-1} for the filter kit of the Bomem FT-Raman instrument that we used, suggests the absence of a low-frequency enhancement effect over the spectral range available, specifically, between ca. 400 and 600 cm^{-1}. It is to be noted that we have corrected for the spectral response of the detector system.

Off-resonance Raman measurements for NTC in various physical states (as shown in Figure 5) strongly suggest that molecular aggregation leads to an enhancement of Raman scattering of vibrational modes of the monomeric species (i.e., intramolecular modes) and an even greater relative enhancement of certain modes of the molecules involved more intimately with formation of the aggregate (i.e., intermolecular modes). Which particular modes are enhanced and the role of excitonic states in the mechanism for enhancement are addressed below. It is clear that SERS arises from a different enhancement mechanism than that operative for aggregation enhancement.

D. Raman Spectra of Reference Compounds. An obvious first step in using Raman spectra to decipher the intermolecular structural geometry of a scattering species that is an aggregate is to determine the vibrational band assignments for the isolated monomeric species. Moreover, vibrational band assignments for the monomer aid in delving into the nature of specific couplings between intramolecular motion and intermolecular degrees of freedom and their impact on possible intensity borrowing interactions.

To gather insight into the nature of vibrational modes of NTC, we have employed an empirical approach in which homogeneous solution phase Raman spectra of reference compounds were correlated to one another. Specifically, correlation of Raman bands of monomeric NTC, mNTC, and NmTA (see Figure 1 for structures) were made and are provided in Table 3; these molecules were chosen as reference compounds to isolate, in a gross fashion, vibrations of NTC that might be assignable to motions of the methine bridge or the aromatic ring system. Column 4 of Table 3 provides such assignments.

The above correlations of Raman bands and their deduced group vibrational assignments provide a reasonable starting point to aid in the assessing of aggregate structure and the nature of vibronic coupling within the aggregate environment.

TABLE 3: Assignment of Raman Bands of Monomeric NTC

NTC[a]	NmTA[a]	mNTC[a]	assignment[b]
175(0.05)		160(0.01)	ν(methine bridge)
–	198(0.17)		
–		224(0.16)	ν(C−C) or $\delta(C-H)_{9R}$
271(0.01)	267(0.10)	265(0.08)	$(ring)_{N-B}$
299(0.02)			
328(0.01)	318(0.16)	332(0.08)	$(ring)_{N-B}$
356(0.01)			
383(0.02)	374(0.26)	394(0.14)	$(ring)_{N-B}$
–	454(0.12)	437(0.11)	
487(0.14)		497(0.22)	C−C in methine bridge
514(0.08)	502(0.22)	506(0.35)	$(ring)_{N-B}$
549(0.01)	535(0.36)		
571(0.32)		572(0.06)	C−C in methine bridge
599(0.61)		596(0.98)	C−C in methine bridge
632(0.01)?			
651(0.03)		653(0.06)	C−C in methine bridge
706(0.12)		707(0.15)	C−C in methine bridge
723(0.33)		724(0.48)	C−C in methine bridge
–		750(0.09)	
–		–	
819(0.04)		837(0.42)	C−C in methine bridge
855(0.48)		852(0.03)	C−C in methine bridge
865(0.10) sh			
–	898(0.12)		?
912(0.07)		912(0.13)	C−C in methine bridge
1006(0.41)			9−phenyl
1038(0.07)	1024(0.22)	1029(0.32)	$(ring)_N$
1076(0.43)		1077(0.25)	C−C in methine bridge
–	1082(0.17)	1092(0.20)	
1124(0.10)		1126 sh	C−C in methine bridge
1146(0.64)	1146(0.12)	1138(0.75)	$(ring)_{N-B}$
1165(0.12)		1164(0.03)	C−C in methine bridge
1185(0.24)	1174(0.16)	1185(0.11)	$(ring)_N$
–	1214(0.24)	1213(1.20)	
1248(0.56)			
	1261(0.19)	1262(0.24)	
1280(0.39)	1276(0.22)	1283(0.08)	$(ring)_N$
1316(0.41)		1314(0.16)	C−C in methine bridge
1356(0.53)	1345(0.48)	1355(0.49)	$(ring)_{N-B}$
–	1365(1.72)	–	
1396(1.00)	1391(1.00)	1390(1.00)	$(ring)_{N-B}$
1416(0.25)			
1442(0.18)	1437(0.64)	1441(0.18)	$(ring)_N$
1459(0.08)	1499(0.37)	1456(0.07)	$(ring)_N$
1521(0.37)	1515(0.24)	1521(0.26)	$(ring)_N$
1548(0.58)	1552(0.28)	1544(0.38)	
1574(0.29)	–	1572(0.40)	C−C in methine bridge
	1580(0.24)		
1607(0.11)			$(ring)_{N-B}$

[a] NTC, 3,3′-dimethyl-9-phenyl-4,5:4′,5′-dinaphthothiacarbocyanine; mNTC, 3,3′-diethyl-9-methyl-4,5,4′,5′-dinaphthothiacarbocyanine; NmTA, 2-methyl-4,5:4′,5′-dinaphthothiazole. [b] N−R, alkyl group attached to N atom; 9-R, alkyl group attached to 9-position in methine bridge; N, Raman mode internal to isolate naphthothiazolic ring; N−B, naphthothiazolic ring modes involving methine bridge and/or alkyl substituent attached to N atoms.

IV. Assignment of the Raman Spectrum of Monomeric NTC

Detailed normal mode analysis of vibrational bands in Raman spectra of cyanine dyes is a daunting task due to the structural complexity of the cyanines. An early attempt at vibrational mode assignment concentrated on the prototypical cyanine PIC and was based on a normal coordinate analysis of the linear conjugated system $>N^+=CH(CH=CH)_nN<$.[71,72] The use of this simplified structure for the dye obviously leads to a significant loss of structural information concerning the quinolinium end groups, which are, in fact, major factors in determining the vibrational spectrum.

Selected Raman bands of PIC have also been interpreted through comparison with the spectra of naphthalene and

propylene.[73] However, this approach is inherently flawed since intermolecular couplings between the quinolinium end groups and the methine linkage in PIC would be expected to cause shifts in vibrational bands, complicating band assignments.

Another empirical approach has utilized methine linkages of different lengths, with the aim of identifying bands that are associated either (principally) with vibrations of the quinolinium groups or the linkage.[74] However, conformational flexibility, associated with chains of different length, complicates band assignments.

Despite the difficulties with band assignments using an empirical approach, it is expected that Raman bands of NTC can be attributed to certain group vibrational modes if careful selection is made of the reference molecules. We attempted to minimize problems associated with the empirical assignment through the following strategies: (1) In order to study the effects of the aromatic phenyl attached to the methine carbon group (i.e., the 9-phenyl substituent), we compared the Raman features of NTC with its homolog in which only the phenyl group is replaced by the methyl group, while the chain lengths was unchanged (specifically, mNTC; see Figure 1). (2) In order to consider possible conjugation effects between the end rings and the methine chain, a correlation was made of Raman bands of NTC with 2-methyl-β-naphthothiazole (mNTA; see Figure 1). The latter was used to simulate the half moiety of NTC involving both the methine bridge and end group.

From comparisons of bands associated with the various compounds (see Table 3), it is evident that Raman bands can be divided into two groups. One group involves bands close in frequency to those of the reference compounds containing the naphthothiazole moiety. The second group involves bands attributed to vibrations that contain major contributions from motions of the methine bridge and/or the alkyl substituents attached to the N atoms of the naphthothiazolic rings, since no corresponding bands are found in the mNTA molecule. Small differences in the correlated frequencies are associated with the influence of conformation of the NTC molecule on band positions.

In summary, we have associated Raman bands of NTC at ca. 487, 571, 599, 651,706, 723, 819, 855, 912, 1073, 1124, 1165, 1310, and 1574 cm^{-1} with stretching and bending of one or more of the following: (i) the methine bridge, (ii) the methyl and ethyl groups attached to the methine bridge, and (iii) the methyl and ethyl groups attached directly to the N atoms of the end groups.

It is also deduced that Raman bands of NTC observed at 328, 383, 514, 1038, 1185, 1280, 1356, 1396, 1442, 1459, and 1521 cm^{-1} (see Tables 3), which are found in the Raman spectra of naphthothiazoles, at nearly the same frequencies, are likely attributable to skeletal vibrational modes of the naphthothiazolic rings (isolated from interaction with *N*-alkyl substituents and/or conjugation with the methine bridge). A further deduction arises from the observation that Raman bands that occur at the same frequencies for NTC, but are shifted (either up- or down-shifted) in the case of mNTC, such as NTC Raman bands at 328, 383, 1146, 1185, 1356, 1442, 1459 and 1552 cm^{-1}, are likely attributable to vibrational modes of the naphthothiazolic ring that also involve the methine bridge and/or *N*-alkyl group motions. Finally, the strong band for NTC at 1006 cm^{-1} is assigned to the internal vibration of the 9-phenyl group.

V. Structure of Aggregated NTC and the Mechanism of Aggregation-Induced Enhanced Scattering

Examination of the data in Table 3 reveals that essentially all Raman features observed in the high-frequency region for NTC monomer, with minor position shifts and relative intensity changes, are present in the Raman spectrum of the aggregate. Moreover, Table 3 reveals that, in the low-frequency region, the Raman spectrum of the aggregate has bands that are absent or weakly present in the spectrum of the monomer, and the relative intensities of all the low-frequency bands (compared to the intensity of bands in the high frequency region) are enhanced, when referenced to the spectrum of the monomer.

The presence of essentially unaltered Raman bands of monomeric NTC in the spectrum of the aggregate suggests the absence of significant structural distortion in NTC upon aggregation. The presence of enhanced low-frequency bands for aggregated NTC thus must be attributed to intermolecular vibrational modes relating to vibrations, probably, in the aggregate formation direction, i.e., lattice modes.

The experimentally derived assertion that lattice modes likely play a decisive role in the emergence of low-frequency enhanced Raman bands for aggregated species is precisely the conclusion reached through the AERS quantum theoretical scheme that we have advanced, which explains the occurrence of various vibrational Raman bands as well as enhancement of intensities for aggregated molecules.[19,25,26]

The AERS scheme indicates that the aggregate's polarizability can be expressed as $\alpha_{ij}^{gv',gv''} = A + B$, where *i* and *j* represent polarization directions, g indicates the ground electronic state, and v′ and v″ refer to upper and lower vibrational states in the scattering problem. The A term has been shown to be principally responsible for the dramatic relative intensity enhancement, upon resonance excitation, of a few low-frequency bands; these enhanced bands (i.e., A term bands) have been found to have half-widths nearly twice that of bands (not enhanced) whose intensities are essentially independent of whether off-resonance or resonant excitation are used, i.e., B term bands. Examination of the Raman spectrum of NTC reveals that several bands, including bands at ca. 133 and 176 cm^{-1}, qualify as A term bands.

The A term of the polarizability has been shown to explicitly involve an additivity factor *N* (the effective number of molecules in the aggregate), energy differences relative to the excitation frequency that lead to absorption resonances, and a factor consisting of sums over excited vibronic states of overlap integral products such as $\langle\chi_{g,v'}|\chi_{r,v}\rangle\langle\chi_{r,v}|\chi_{g,v''}\rangle$ where χ's are the vibrational wave functions and r,v represents an excited vibronic state of the scattering species.[21] Included among the available excited vibronic states are excited-state lattice modes of the aggregate resulting from the intermolecular potential function. These latter vibrations have intercalated within them the intramolecular, single-molecule vibrations and, as a result, would be expected to yield nonzero overlap integrals with appropriate intramolecular vibrations.[20,21,23]

The B term has been shown to lead to Raman intramolecular vibrational bands. This latter deduction arose through the application of several approximations, including Herzberg−Teller intensity borrowing from allowed transitions and the use of vibrational closure relationships in the off-resonance situation.[19,21,75] Within the harmonic oscillator approximation, in fact, all B term bands are fundamentals.[19]

An important approximation that enabled association of the A term with specific vibrational motions was the assumption of the "strong-coupling" case for exciton formation, as discussed by Kasha,[14] which corresponds to little impediment to the excitation roaming through the aggregate structure. The net result of this assumption is that the associated A term cannot contribute to the appearance of Raman bands resulting from the overlap of intramolecular ground and intramolecular vi-

broexcitonic modes: the electronic excitation would be spread over many molecules, resulting in each molecule having essentially the same electronic structure as a ground-state molecule and, as a result of the Franck−Condon principle, zero vibrational overlap integral products between excited- and ground-state levels.[76] However, there is no Franck−Condon proscription for nonzero overlap integral products between vibrationally excited lattice modes of the aggregate (i.e., intermolecular vibrations) and ground-state intramolecular modes. Thus, the Raman modes in the AERS scheme that are excited through this term are likely ones with substantial motion in the aggregate formation direction, i.e., perpendicular to the naphthothiazole moiety.

Appropriate excited-state lattice modes, which can be represented by a superposition of appropriate single-molecule intramolecular modes, may possess nonzero vibrational overlap integral products with ground-state intramolecular modes as required for nonvanishing of the A term.[25]

The characteristics of the Raman spectrum of aggregated NTC is consistent with that predicted by the AERS mechanism and provides further evidence, in addition to that provided by our earlier investigations,[21,36,37] for the correctness of the inculcated theoretical concepts.

The fact that two intense low-frequency A term bands (the bands at ca. 133 and 176 cm^{-1}) exist is suggestive, based on our earlier determinations, of the presence of two types of NTC J-aggregates. Preliminary molecular modeling calculations in this laboratory for the monomer indicate a twisted structure in which the naphthothiazole rings are not coplanar. Hence, obvious candidates for the two structures would be right and left helical arrangements. However, J-aggregates composed of two different ground-state stereoisomers are also a strong possibility, especially so given the decrease in fluorescence lifetime of the monomeric species with decrease in the viscosity of the solvent that we have measured (*vide supra*). Further investigations in this laboratory, both experimental measurements and (especially) quantum structure calculations, will seek to determine more about the structure of the aggregates.

VI. Conclusions

Absorption and fluorescence lifetime measurements confirm that NTC forms aggregates in homogeneous solution. Empirical vibrational bands assignments for aggregated NTC have been obtained by correlating Raman spectra of NTC and reference compounds in their monomeric states. Off-resonance Raman investigations have led to vibrational band assignments that suggest that monomeric NTC maintains its structural integrity in the aggregate environment—as suggested by only minor changes in the frequencies of Raman bands. Resultant assignments of vibrational bands to motions of various moieties of NTC provide a basis for discussion of the influence of the aggregate environment on relative band shifts and for deducing that out-of-plane vibrations play a pivotal role in giving rise to enhanced vibrational band intensities, especially for low-frequency modes, which the AERS mechanism for enhancement identifies as originating from the A term of the polarizability. The present experiment confirms the viability of the AERS mechanism.

References and Notes

(1) Pearlstein, R. M. In *Photosynthesis*; Amesz, J., Ed.; Elsevier: Amsterdam, 1987; pp 299−317.
(2) Warshel, A.; Parson, W. W. *J. Am. Chem. Soc.* **1987**, *109*, 6143, 6152.
(3) Creighton, S.; Hwang, J.-K.; Warshel, A.; Parson, W. W.; Norris, J. *Biochemistry* **1988**, *27*, 774.
(4) Michel-Beyerle, M. E., Plato, M.; Deisenhofer, J.; Michel, H.; Bixon, M.; Jorter, L. *Biochem. Biophys. Acta* **1988**, *932*, 52.
(5) Gilman, P. B. *Photo. Sci. Eng.* **1974**, *18*, 418.
(6) Borsenberger, P. M.; Chowdry, A.; Hoesterey, D. C.; Mey, W. *J. Appl. Phys.* **1978**, *44*, 5555.
(7) Waggoner, A. *J. Membrane Biol*. **1976**, *27*, 317.
(8) Chatterjee, S.; Davis, P. D.; Gottschalk, P.; Kurz, M. E.; Sauerwein, B.; Yang, X.; Schuster, G. B. *J. Am. Chem. Soc.* **1990**, *112*, 6329.
(9) Hanamura, E. *Phys. Rev. B.* **1988**, *37*, 1273.
(10) Sasaki, F.; Kobayashi, S. *Appl. Phys. Lett.* **1993**, *63*, 2887.
(11) Wang, Y. *Chem. Phys. Lett.* **1986**, *126*, 209.
(12) Wang, Y. *J. Opt. Soc. Am. B* **1991**, *8*, 981.
(13) Kobayashi, S. *Mol. Cryst. Liq. Cryst.* **1992**, *217*, 77.
(14) Kasha, M. *Radiation Res.* **1963**, *20*, 55.
(15) Sturmer, D. M.; Heseltine, D. W. In *The Theory of the Photographic Process*, 4th ed.; James, T. H., Ed.; MacMillian Publishing Co.: New York, 1977; Chapter 8.
(16) Herz, A. H. *Adv. Colloid Interface Sci.* **1977**, *8*, 237.
(17) Mobius, D.; Kuhn, H. *Isr. J. Chem.* **1979**, *18*, 375.
(18) Mobius, D. *Acc. Chem. Res.* **1981,** *14*, 63.
(19) Akins, D. L. *J. Phys. Chem.* **1986**, *90*, 1530.
(20) Akins, D. L.; Lombardi, J. R. *Chem. Phys. Lett.* **1987**, *136*, 495.
(21) Akins, D. L.; Akpabli, C. K.; Li, X. *J. Phys. Chem.* **1989**, *93*, 1977.
(22) Akins, D. L.; Macklin, J. W. *J. Phys. Chem.* **1989**, *93*, 5999.
(23) Akins, D. L.; Macklin, J. W.; Parker, L. A.; Zhu, H.-R. *Chem. Phys. Lett.* **1990**, *169*, 564.
(24) Akins, D. L.; Macklin, J. W.; Zhu, H.-R. *J. Phys. Chem.* **1991**, *95*, 793.
(25) Akins, D. L.; Zhu, H.-R. *Langmuir* **1992**, *8*, 546.
(26) Akins, D. L.; Zhuang, Y. H.; Zhu, H.-R.; Liu, J. Q. *J. Phys. Chem.* **1994**, *98*, 1068.
(27) Selwyn, J. E.; Steinfeld, J. I. *J. Phys. Chem.* **1972**, *76*, 762.
(28) Ojeda, P. R.; Amashta, I. A. K.; Ochoa, J. R.; Arbeloa, I. L. *J. Chem. Soc., Faraday Trans. 2* **1988**, *84*, 1.
(29) Valdes-Aguilera, O.; Neckers, D. C. *Acc. Chem. Res.* **1989**, *22*, 171.
(30) Kasha, M.; Rawls, H. R.; El-Bayoumi, M. A. *Pure Appl. Chem.* **1965,** *11*, 37.
(31) Hessemann, J. *J. Am. Chem. Soc.* **1980**, *102*, 2167, 2176.
(32) Vincent, P. S.; Barlow, W. A. *Thin Solid Films* **1980**, *71*, 305.
(33) Fukuda, K.; Nakahara, H. *J. Colloid Interface Sci.* **1984**, *98*, 555.
(34) Mooney, W. F.; Brown, P. E.; Russel, J. C.; Costa, S. B.; Pederson, L. G.; Whitten, D. G. *J. Am. Chem. Soc.* **1984**, *106*, 5659.
(35) Mooney, W. F.; Whitten, D. G. *J. Am. Chem. Soc.* **1986**, *108*, 5712.
(36) Akins, D. L.; Zhu, H.-R.; Guo, C. *J. Phys. Chem.* **1994**, *98*, 3612.
(37) Akins, D. L.; Zhu, H.-R.; Guo, C. *J. Phys. Chem.* **1996**, *100*, 5420.
(38) Akins, D. L.; Özçelik, S.; Zhu, H.-R.; Guo, C. *J. Phys. Chem.* **1996**, *100*, 14390.
(39) (a) Czikkely, V.; Dreizler, G.; Forsterling, H. D.; Kuhn, H.; Sondermann, J.; Tillman, P.; Wiegand, J. *Z. Naturforsch.* **1969**, *24A*, 1821. (b) Czikkely, V.; Forsterling, H. D.; Kuhn, H. *Chem. Phys. Lett.* **1970**, *6*, 11. (c) Briggs, J. S.; Herzenberg, A. *Mol. Phys.* **1971**, *21*, 865. (d) Hemenger, R. P. *J. Chem. Phys*. **1976**, *66*, 1795. (e) Fulton, R. L.; Gouterman, M. *J. Chem. Phys.* **1961**, *35*, 1059. (f) Fulton, R. L.; Gouterman, M. *J. Chem. Phys.* **1964**, *41*, 2280. (g) Kopainsky, B.; Hallermier, J. K.; Kaiser, W. *Chem. Phys. Lett.* **1981**, *83*, 498. (h) Kopainsky, B,; Hallermier, J. K.; Kaiser, W. *Chem. Phys. Lett.* **1982**, *87*, 7.
(40) (a) Kopainsky, B.; Hallermier, J. K.; Kaiser, W. *Chem. Phys. Lett.* **1981**, *83*, 498. (b) Kopainsky, B.; Hallermier, J. K.; Kaiser, W. *Chem. Phys. Lett.* **1982**, *87*, 7. (c) Scherer, P. O. J.; Fischer, S. F. *J. Chem. Phys*. **1984**, *86*, 269. (d) Knapp, E. W.; Scherer, P. O. J.; Fischer, S. F. *Chem. Phys. Lett*. **1984**, *111*, 481. (e) Knapp, E. W.; Fischer, S. F. *Chem. Phys. Lett.* **1984**, *103*, 479. (f) Knapp, E. W. *Chem. Phys*. **1984**, *85*, 73. (g) Knapp, E. W. *Chem. Phys. Lett.* **1984**, *108*, 342.
(41) (a) Spano, F. C.; Mukamel, S. *J. Chem. Phys*. **1989,***91*, 683. (b) Grad, J.; Hernandez, G.; Mukamel, S. *Phys. Rev. A* **1988**, *37*, 3835.
(42) (a) Spano, F. C.; Kuklinski, J. R.; Mukamel, S. *Phys. Rev. Lett.* **1990**, *65*, 211. (b) Spano, F. C.; Mukamel, S. *Phys. Rev*. **1989**, *40a*, 5783.
(43) Scheibe, G.; Mareis, A.; Schiffmann, R. *Z. Physik. Chem. B* **1941**, *49*, 324.
(44) Rosenoff, A. E.; Walworth, V. K.; Bird, G. R. *Photogr. Sci. Eng.* **1970**, *14*, 328.
(45) Emerson, E. S.; Conlin, M. A.; Rosenoff, M. A.; Norland, K. S.; Rodriguez, H.; Chin, H.; Bird, G. R. *J. Phys. Chem*. **1967**, *71*, 2396.
(46) Buecher, H.; Kuhn, H. *Chem. Phys. Lett*. **1970**, *6*, 183; Czikkely, V.; Fösterling, H. D.; Kuhn, H. *Chem. Phys. Lett*. **1970**, *6*, 207.
(47) Akins, D. L. In *J-Aggregates;* Kobayashi, T., Ed.; World Scientific: Singapore, 1996; Chapter 3, pp 67−94.
(48) De Boer, Steven; Vink, Dees J.; Wiersma, Douwe A. *Chem. Phys. Lett.* **1987**, *137*, 99.
(49) De Boer, Steven; Wiersma, Douwe A. *Chem. Phys. Lett.* **1990**, *165*, 45.
(50) Fidder, H.; Knoster, J.; Wiersma, D. A. *Chem. Phys. Lett.* **1990**, *171*, 529.

(51) Fidder, H.; Terpstra, J.; Wiersma, D. A. *J. Chem. Phys.* **1991**, *94*, 6895.
(52) De Boer, S.; Wiersma, D. A. *Chem. Phys.* **1989**, *131*, 135.
(53) Akins, D. L.; Macklin, J. W.; Zhu, H.-R. *J. Phys. Chem.* **1992**, *96*, 4515.
(54) West, W.; Pearch, S. *J. Phys. Chem.* **1965**, *69*, 1894.
(55) O'Brien, D. F.; Kelly, T. M.; Costa, L. F. *Photo. Sci. Eng.* **1974**, *18*, 76.
(56) Knudtson, J. T.; Eyring, E. M. *J. Phys. Chem.* **1974**, *78*, 2355.
(57) Tredwell, C. J.; Keary, C. M. *Chem. Phys.* **1979**, *43*, 307.
(58) Sundström, V.; Gillbro, T. J. *Chem. Phys.* **1985**, *83*, 2733.
(59) Murphy, S.; Sauerwein, B.; Drickamer, H. G.; Schuster, G. B. *J. Phys. Chem.* **1994**, *98*, 13476.
(60) Aramendia, P. F.; Negri, R. M.; San Romàn, E. *J. Phys. Chem.* **1994**, *98*, 3165.
(61) Awad, M. M.; McCarthy, P. K.; Blanchard, G. J. *J. Phys. Chem.* **1994**, *98*, 1454.
(62) Åkesson, E.; Sundström, V.; Gillbro, T. *Chem. Phys.* **1986**, *106*, 269.
(63) Maiti, N.; Ravikanth, M.; Mazumdar, S.; Periasamy, N. *J. Phys. Chem.* **1995**, *99*, 17192.
(64) Yu, Z. X.; Lu, P. Y.; Alfano, R. R. *Chem. Phys. Lett.* **1983**, *79*, 289.
(65) Kopainsky, B.; Kaiser, W. *Chem. Phys. Lett.* **1982**, *88*, 357.
(66) Rentsch, S. K.; Danielius, R. V.; Gadonas, R. A.; Piskarkas, A. *Chem. Phys. Lett.* **1981**, *84*, 446.
(67) Brumbaugh, D. V.; Muenter, A. A.; Knox, W.; Mourau, G.; Wittmershaus, B. *J. Lumin.* **1984**, *31* and *32*, 783.
(68) Fink, F.; Klose, E.; Teuchner, K.; Dahne, S. *Chem. Phys. Lett.* **1977**, *45*, 548.
(69) Sundström, V.; Gillbro, T.; Gadonas, R. A.; Piskarkas, A. *J. Chem. Phys.* **1988**, *89*, 2754.
(70) Gu, B.; Akins, D. L. *Chem. Phys. Lett.* **1985**, *113*, 558.
(71) Mejean, T.; Forel, M. T. *J. Raman Spectrosc.* **1977**, *6*, 117.
(72) Rayez, J. C.; Forel, M. T.; Mejean, T. *J. Raman Spectrosc.* **1980**, *9*, 125.
(73) Pace, J.; Pace, E. L. *Spectrochim. Acta* **1980**, *36A*, 557.
(74) Yang, J. P.; Callender, R. H. *J. Raman Spectrosc.* **1985**, *16*, 319.
(75) Albrecht, A. C. *J. Chem. Phys.* **1961**, *34*, 1476.
(76) Fischer, G. *Vibronic Coupling: The Interaction Between the Electronic and Nuclear Motions;* Academic: New York, 1984.
(77) Reichardt, C. *Solvent Effects in Organic Chemistry*; Verlag Chemie: New York, 1979.